ECS Transactions, 68 (1) 773-784 (2015)
10.1149/06801.0773ecst ©The Electrochemical Society

Investigating the Relationship Between Operating Conditions and SOFC Cathode Degradation

C. Pellegrinelli, Y. L. Huang, J. A. Taillon, L. G. Salamanca-Riba, and E. D. Wachsman

University of Maryland Energy Research Center, University of Maryland College Park, College Park, Maryland 20742, USA

Polarization losses associated with the cathode oxygen reduction reaction and degradation of cathode materials remain as hurdles for widespread implementation of solid oxide fuel cells (SOFC). Rates of degradation depend significantly on the operating temperature and gas conditions, such as the presence of unwanted oxygen-containing compounds, namely H_2O and CO_2. In this study we explore degradation mechanisms for a common composite cathode material, $La_{0.6}Sr_{0.4}Co_{0.2}Fe_{0.8}O_{3-\delta}$ (LSCF) - $Ce_{0.90}Gd_{0.10}O_{1.95}$ (GDC). Three-electrode cells have been tested under various temperatures, PO_2s and contaminant conditions in order to observe changes through electrochemical impedance spectroscopy (EIS). EIS is a powerful tool, which allows us to identify changes in the reaction steps comprising the overall ORR. Our EIS results indicate a strong correlation between blocking effects, caused by CO_2 and H_2O, and the operating temperature of the cell. Using EIS to de-convolute the overall cathode polarization helps to identify the mechanisms by which degradation occurs.

Introduction

Solid oxide fuel cells (SOFCs) are a promising technology for the generation of electricity through the electrochemical oxidation of fuels (1-3). However, there are key challenges remaining for the widespread use of SOFCs, most notably high polarization losses associated with the oxygen reduction reaction that occurs at the cathode, and the degradation of cathode materials under contaminant environments. The contributions of the cathode to overall polarization losses are derivative of the mechanistic steps involved in the ORR.

Some of the most common and promising cathode materials for SOFCs are LSM ($La_{1-x}Sr_xMnO_3$) and LSCF ($La_{1-x}Sr_xCo_yFe_{1-y}O_{3-\delta}$). LSM is an electron conducting oxide that is highly catalytic toward the ORR. However, LSM provides limited oxygen ion conductivity, confining reactions to the triple phase boundary (TPB) region where oxygen gas, cathode and electrolyte meet, and restrict LSM to high temperature operation. On the other hand, LSCF is a mixed ionic-electronic conductor (MIEC) that has promise as an SOFC cathode for the intermediate temperature range. With the ability to conduct ions and electrons, LSCF can extend the active region of the cathode beyond the TPB (4). However, there are still a number of factors limiting the performance of LSCF, namely the instability of the material in typical operating environments, which often contain water vapor and CO_2 (5-7). The presence of CO_2 and water vapor can cause

significant degradation in LSCF through the formation of secondary phases, such as SrO. It has been proposed that the presence of these contaminants will increase surface decomposition by reducing the number of sites available for oxygen reduction and the formation of $SrCO_3$, in the case of CO_2 (8). In addition, lowering of operating temperatures may increase the detrimental effects of the contaminants (9).

Electrochemical impedance spectroscopy (EIS) is a powerful tool that allows us to identify changes in conductivity for the reaction steps comprising the overall ORR. EIS can provide information about bulk, interfacial, and chemical properties of the material through proper analysis (10-14). We have developed a strategy for identifying the steps in the ORR that contribute to the overall impedance spectra, and how each contribution changes as a function of operating conditions and aging time. In this investigation we used EIS to determine the effects of the common cathode contaminants, water and CO_2, on the ORR kinetics and material stability of LSCF-GDC (50% weight $La_{0.60}Sr_{0.40}Co_{0.20}Fe_{0.80}O_{3-x}$ - 50% weight $(Ce_{0.90}Gd_{0.10})O_{1.95}$) composite cathodes. Our previously reported gas phase isotope exchange data indicates a strong interaction between water and LSCF powders near 450°C, with decreasing exchange as the temperature was increased up to 800°C (15). Based on these results, cells were aged in water environments at both 450°C and 750°C and impedance spectra were recorded as a function of aging time. LSCF-GDC three-electrode cells were also tested under CO_2 environments at both 450 and 750°C. However, gas phase isotope exchange data showed a strong interaction of LSCF with CO_2 across the entire temperature range studied, from 100 to 800°C (15). In addition, impedance spectra were gathered under a wide range of conditions to determine the dependence of the various contributions to impedance as a function of testing conditions (i.e. temperature, PO_2, PCO_2).

Experimental

LSCF-GDC/GDC/LSCF-GDC symmetrical cells were fabricated for electrochemical testing. $Gd_{0.10}Ce_{0.90}O_{2-x}$ powder (Fuel Cell Materials) was uniaxially pressed in a 10mm diameter die and sintered at 1450°C for 6 hours. The sintered pellets were then ground to a thickness of 5mm, and a thin groove was cut along the center of the pellet (2.5mm from both the top and bottom) for placement of a reference electrode. Subsequently, LSCF-GDC composite cathode paste (Fuel Cell Materials) was printed on the top and bottom of the GDC pellets and then sintered at 950°C for 2 hours. Pt paste was painted inside the previously cut groove and a Pt wire wrapped around the pellet, held in place by the groove, to act as a reference electrode. The Pt paste was dried at 900°C for 30 min. Finally, a thin layer of Au paste was painted on both the working and counter electrodes and dried at room temperature for 1 hour. The cells were then loaded into a custom built single-environment reactor and heated to 875°C for 15 minutes to finish drying the Au paste before being cooled to the temperature of interest to begin testing. An image of an as-prepared LSCF-GDC/GDC/LSCF-GDC cell before painting on Au paste, and an SEM image of the LSCF-GDC/GDC interface is shown in Figure 1.

EIS measurements were performed using a 1400 Frequency Response Analyzer and a 1470 Cell Test System (Solartron Analytical). During aging tests, cells were held at a constant temperature, in a constant gas environment, and EIS spectra measured throughout the aging process. A thermocouple was placed inside the reactor, near the cell

to ensure accurate temperature measurements. Gas flow rates and mixtures were controlled using a set of mass flow controllers (MKS). Aging studies were performed at an O_2 concentration of 20%, with either 5% CO_2, controlled by a mass flow controller, or 3% H_2O, introduced through a glass impinger at room temperature. Cells aged at 750°C were aged for 500 hours, while cells aged at 450°C were cooled after 350 hours. All samples were aged and EIS spectra measured, under open circuit voltage. Post-analysis X-ray diffraction of cells was performed with a Bruker D8 Advance, Cu K_α.

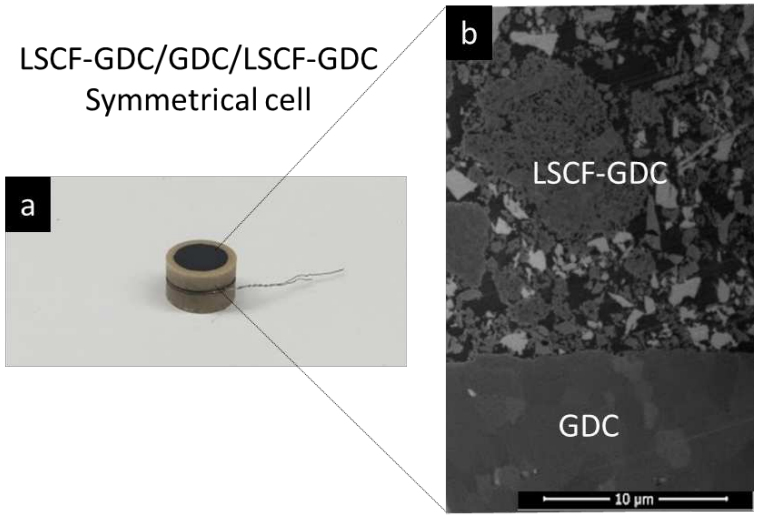

Figure 1. (a) LSCF-GDC/GDC/LSCF-GDC three-electrode symmetrical cell, as fabricated. (b) SEM imaged of LSCF-GDC interface.

Results and Discussion

A common degradation mechanism for LSCF is the formation of secondary phases, namely SrO. This is especially true for LSCF aged in the presence of CO_2, as it is believed that strontium carbonate ($SrCO_3$) is an effective intermediate for Sr segregation (16, 17). Figure 2a-b shows the result of x-ray diffraction (XRD) on cells aged in 20%O_2 with the presence of CO_2 and H_2O, at 450°C and 750°C. The presence of LSCF, GDC and Au is seen in the diffraction pattern, but no secondary phases are discernable. It is possible that the resolution of XRD is such that a small amount of surface segregates will not be detected. While the total amount of segregation may be small compared to the bulk of the cathode material, degradation of the surface can have significant effects on the performance of the material. EIS can give insight into the surface properties of LSCF-GDC cathodes that *ex-situ* post-analysis techniques may not be able to provide.

EIS Fitting and De-convolution

In order to understand the effects of contaminants and aging on LSCF-GDC composite cathodes, a discussion of the analysis of EIS data is necessary. It is crucial to develop a reliable global equivalent circuit to quantitatively describe the degradation mechanisms of CO_2 and H_2O. Figures 2a-d show Bode plots for three-electrode cell measurements between 450°C and 750°C. The impedance spectra shown are for an

LSCF-GDC cell in 20%O_2, balance N_2, prior to aging. Looking at the evolution of the impedance spectra as a function of temperature we can identify changes that occur in the various arcs. At 450°C there appear to be at least two distinct arcs, one with a peak frequency of 1kHz and a second lower frequency arc with a peak near 3Hz. As the temperature of the cell is increased to 550°C, 650°C and finally 750°C, we can see thatthe sizes of both the high and low frequency arcs are decreasing. The low frequency arc, with a characteristic frequency of 3Hz, in comparison to the high frequency arc, appears to be decreasing more rapidly, suggesting that the low frequency arc may contain the rate-limiting surface exchange step, due to it's higher activation energy. In addition one can see a shift to higher characteristic frequencies for both the low and high frequency arcs, which can be expected.

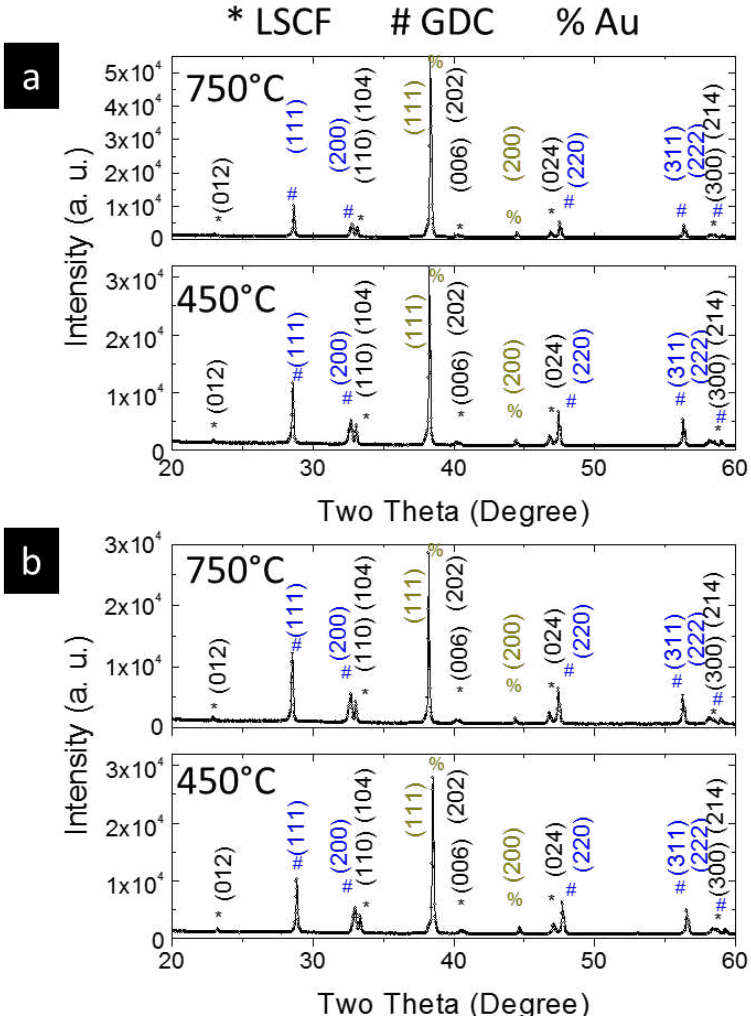

Figure 2. X-ray diffraction of LSCF-GDC/GDC/LSCF-GDC symmetrical cells after aging in (a) 3%H_2O and (b) 5%CO_2 at both 450°C and 750°C. No secondary phases are discernable from the diffraction data under any of the tested conditions.

In addition to the two distinct arcs present for all four temperatures, there is a significant contribution of inductance in the high frequency region, most likely due to the reactor set-up and the high temperature operation of the cell. Although the inductance

does not provide any directly useful information about the cells themselves, it is important to consider the impact inductance can have on extracting quantitative information through fitting programs. In order to minimize the effects of inductance on "real" cell components, a constant inductance value is added to the equivalent circuit to fit all aging data. To establish a robust and consistent fitting process all aging data has been fit using ZSimpWin (EChem Software). The equivalent circuit used to fit the data is shown in Figure 4a and is composed of three main parts. First, there is a series inductor to account for the inductance caused by the high temperature set-up, followed by a resistor in series. Typically, the series resistor is attributed to the overall resistance of the electrolyte, both bulk and grain boundary, and can be denoted R_Ω. Finally, there are two resistor-constant phase element parallel pairs (R-CPE) following, in series. The R-CPE parallel component provides both capacitive and resistive information about charge transfer processes. At high temperature we also often see the growth of a third arc. Due to the low frequency nature, and growth at high temp and low PO_2, we attribute this arc to gas diffusion, and therefore do not consider it in our analysis.

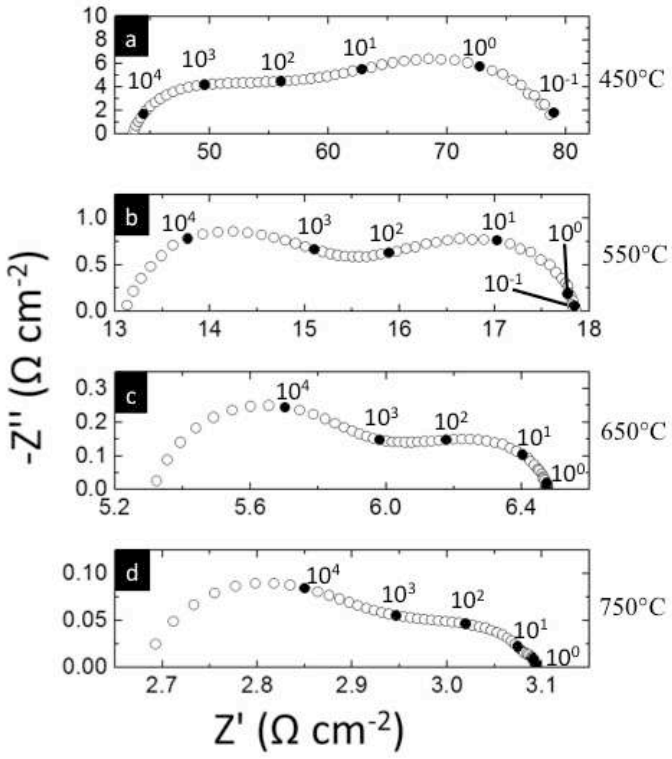

Figure 3. Nyquist plots for LSCF-GDC three-electrode cells at (a) 450°C, (b) 550°C, (c) 650°C, (d) 750°C. There appear to be at least two arcs present across the whole temperature range. The lower frequency arc appears to be decreasing more than the high frequency arc as temperature increases.

The equivalent circuit shown in Figure 4a provides the fits shown in Figures 3b-c, for LSCF-GDC cells at 450 and 750°C respectively (18). Utilizing the circuit shown, one can maintain fit results with errors of less than 1%, providing reliable quantification of parameters. Fitting results provide information about the characteristic frequencies and capacitances of the arcs, which help to determine what the various contributions to the

impedance are. In addition, one can look at how the resistance of each contribution changes as a function of operating conditions and time.

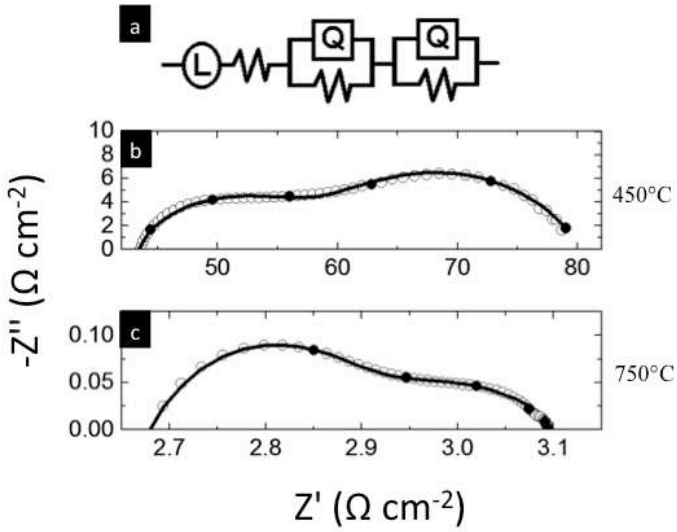

Figure 4. All impedance spectra have been fit with (a) the equivalent circuit using ZSimpWin, never exceeding overall fitting errors greater than 1%. Also shown are representative impedance spectra (symbols) for (b) 450°C, and (c) 750°C and calculated fitting values (line).

Figure 5a-b is representative plots of R_{Ω}, R_{HF}, and R_{LF} as functions of temperature. In Figure 5a one can see the Arrhenius dependence for the ohmic portion of the measured impedance spectra. The conductivity clearly increases as a function of temperature, with an activation energy of ~66kJ/mol. This is in close agreement with literature values for the Arrhenius dependence of the GDC electrolyte. Xia et al. (19) reports an activation energy of 65.5 kJ/mol and Steele (20) reports a value of 64 kJ/mol. Further, we can see from Figure 5b how the resistance of the high and low frequency arcs, R_{HF} and R_{LF}, change with temperature. The plot shows that R_{HF} has an activation energy of ~70kJ/mol while R_{LF} has a higher activation energy of ~100kJ/mol. Using Equation [1], where R is the resistor value, Q the capacitive portion of the CPE, and n the depression of the CPE arc, in a R-CPE parallel circuit component, we can extract C_{eq}, an equivalent capacitance of the circuit component. Understanding the value of the equivalent capacitance can provide information on the type of process occurring.

$$C_{eq} = \frac{(RQ)^{\frac{1}{n}}}{R} \qquad [1]$$

C_{eq} values for the high frequency arc are on the order of 10^{-5}F, indicating that this is likely a double layer effect, i.e. the interface of two materials. R_{HF} may therefore be attributed to interfacial resistance between the LSCF and GDC phases. The low frequency arc has C_{eq} values a couple orders of magnitude lower, at approximately 10^{-3}F, more closely associated with chemical processes. One can therefore attribute the low

frequency arc to chemical reaction processes between oxygen gas and the cathode. Therefore, this work will now refer to the R_{HF} and R_{LF} as R_{int} and R_{chem}, respectively.

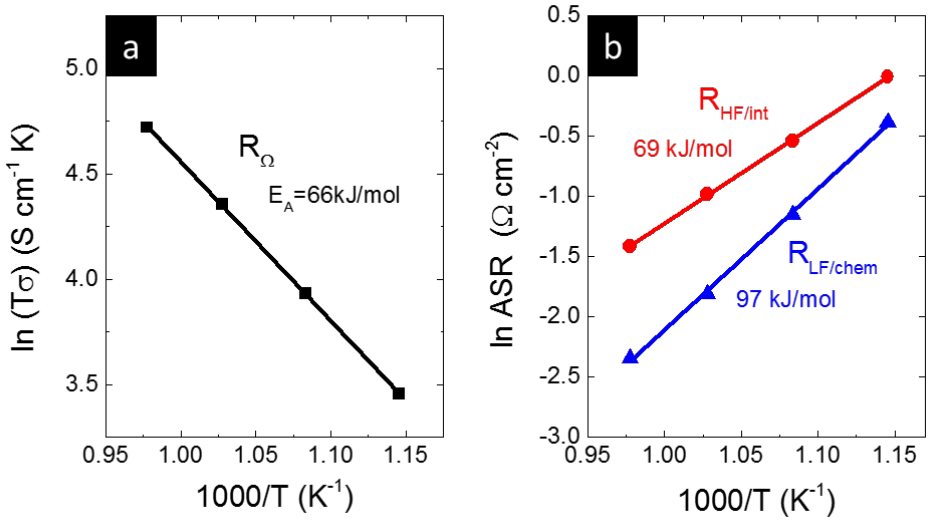

Figure 5. Representative Arrhenius plots for the (a) ohmic, (b) higher frequency, and lower frequency contributions to the impedance spectra. The activation energy for R_{Ω} is ~66kJ/mol, which is in agreement with literature values (19, 20). The high frequency arc, R_{HF}, has a lower temperature dependence than the lower frequency arc, with an apparent activation energy of ~70kJ/mol. R_{LF} has an apparent activation energy of 100kJ/mol. The capacitance values and temperature dependence indicates that R_{HF} may be attributed to interfacial processes, while R_{LF} can be attributed to chemical process (i.e. ORR).

Effects of H_2O

Figure 6 is an Arrhenius plot showing the effects of the presence of 3% H_2O on R_{int} and R_{chem}. There is almost no change in R_{int} across the entire temperature range. In contrast, R_{chem} appears to increase in resistance due to 3%H_2O. The increase in R_{chem} is more prevalent at 450 and 550°C than at higher temperatures. This results in an increase of the activation energy of R_{chem} for this cell from 97kJ/mol to 111kJ/mol. The results indicate that the presence of 3%H_2O impacts how O_2 interacts with the surface of LSCF, impeding the overall ORR.

This result is in strong agreement with results obtained from gas phase isotope exchange data. Isotope saturated temperature programmed exchange (ISTPX), a detailed description of which is provided in (15), shows that the presence of water tends to decrease the exchange between O_2 and LSCF at lower temperatures (300-500°C), an effect that becomes less prevalent at higher temperature (500-800°C). From EIS and ISTPX one can see that the effect of water at low temperature is relatively quick, indicating that blocking of O_2 surface reaction sites is highly likely.

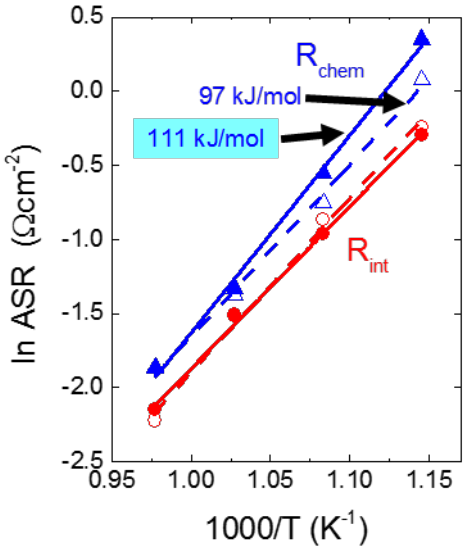

Figure 6. Arrhenius plots for LSCF-GDC cells in 20% O_2 with (closed symbols, solid lines) and without (open symbols, dashed lines) 3%H_2O. There is a clear increase in the activation energy of R_{chem} from ~97kJ/mol to ~111kJ/mol, caused by increased resistance as temperature decreases.

EIS spectra of cells aged in 3%H_2O at 450 and 750°C are shown in Figures 6a-c. 3%H_2O has almost no impact on the cell aged at 450°C. Figure 7a shows Nyquist plots for 0 and 350 hours of aging time at 450°C with 3%H_2O, where there is negligible change in the impedance spectra. However, for LSCF-GDC cells aged at 750°C in 3%H_2O, Figure 7b, a change is observed in the cell's impedance spectra. First, there is an increase in R_Ω as a function of aging time. This increase in R_Ω is accompanied by a slight decrease in R_{int} and a slight increase in R_{chem}. Fitting results for selected aging times are shown in Figure 7c. The equivalent circuit discussed previously, Figure 4a, was used to extract values for R_Ω, R_{int}, and R_{chem}. The majority of the increase in R_Ω occurs between 0-400hours and begins to level off slightly afterwards. In addition, small changes were observed in R_{int} and R_{chem}. Overall, aging in 3%H_2O at 750°C appears to mostly impact the ohmic portion of the impedance. This may be a result of the high temperature, and less likely due to the presence of water. However, it has been proposed that humidity in the presence of other electrolyte materials, namely yttria stabilized zirconia (YSZ), can cause significant degradation and cannot be fully ruled out (21-23).

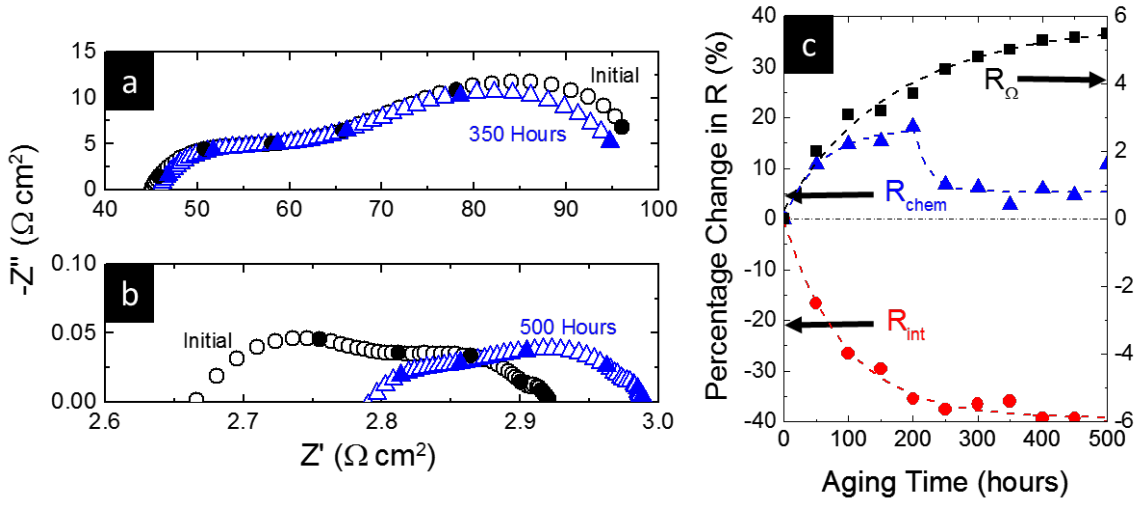

Figure 7. Impedance spectra for LSCF-GDC cells aged in 20%O_2 and 3%H_2O at (a) 450°C and (b) 750°C. For the cell aged at 450°C there is almost no change after 350 hours of aging in 3%H2O. In contrast at 750°C there is a significant change in both R_Ω and R_{int}. The change in these two parameters is likely a result of sintering effects from the high temperature operation. The percent change in the individual parameters is shown in (c).

Effects of CO_2

The performance and stability of LSCF-GDC cathodes was also tested with the presence of CO_2. Figure 8a-c shows Nyquist plots for cells aged in 5%CO_2 at 450 and 750°C. At 450°C, shown in Figure 8a, there is little to no change in R_Ω and R_{int}. However, there is a steady increase in R_{chem} at this temperature. Although R_{chem} does grow significantly with the presence of 5%CO_2, after 250 hours of aging, the flow of CO_2 is ceased, flowing only 20% O_2 balanced in N_2, resulting in a rapid decrease in the size of R_{chem}. At 450°C it appears that the presence of CO_2 can play a significant role in the overall polarization of the cell. However, further results show the effect of CO_2 can be considered reversible; after only 30 minutes of 0% CO_2, the size of R_{chem} is almost completely reversed back to what it was before the introduction of CO_2. In addition, some assumptions can be made about the mechanism of CO_2 interaction with LSCF-GDC based on these results. Due to the gradual increase in R_{chem} with time, it is likely that CO_2 is loading onto the surface of the cathode, blocking sites for O_2 to adsorb on. This low temperature process may be very important as the operating temperature of SOFCs is decreased. Figure 8b demonstrates the aging of LSCF-GDC in 5%CO_2 at 750°C. For this temperature, there are changes in the size of R_{int} and a shift to higher values in R_Ω. The size of R_{chem}, however, appears to stay constant throughout the entire aging process, even after stopping the flow of 5% CO_2. The trends for R_Ω, R_{int}, and R_{chem} are shown in Figure 8c for aging at 750°C.

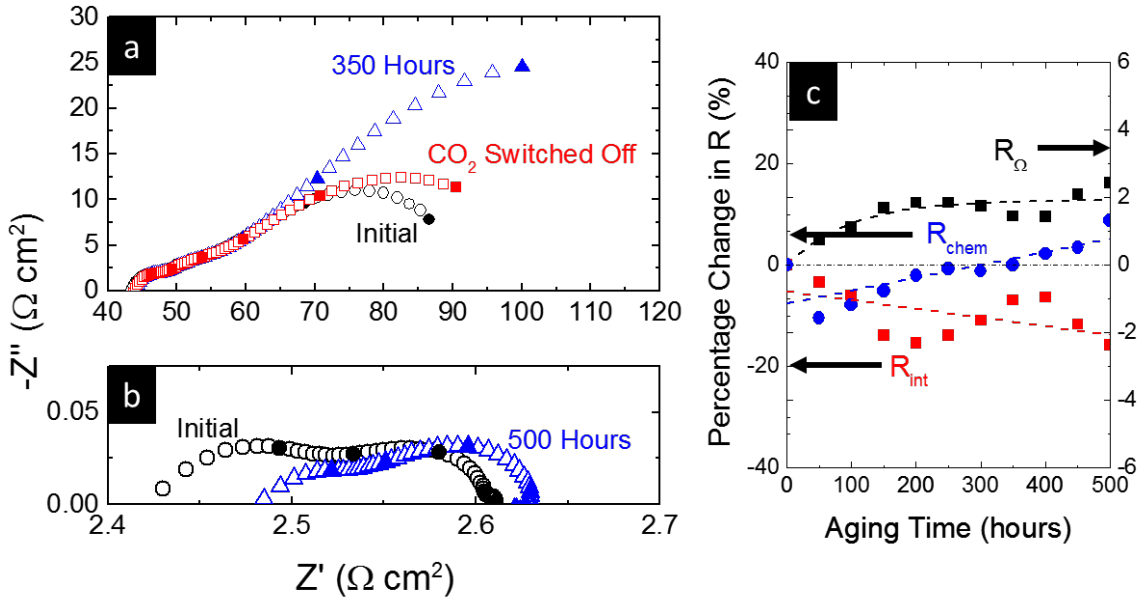

Figure 8. Impedance spectra for LSCF-GDC cells aged in 20% O_2 and 5% CO_2 at (a) 450°C and (b) 750°C. At 450°C R_{chem} increases gradually with aging time. After aging for 350 hours at 450°C, CO_2 flow to the cell was shut off and within 30 minutes the large increase in R_{chem} is almost completely reversed. At 750°C there is an increase in R_Ω and a decrease in R_{int}. The resistance trends are shown in (c). Similar to the cell aged in water at 750°C, these changes are likely due to cathode sintering effects.

Figure 9 shows the temperature dependence of LSCF-GDC before and after aging, as well as after aging with the presence of 5% CO_2. From the fit lines apparent activation energy for R_{int} and R_{chem} are extracted to observe how this activation energy is affected by aging. For all three cases, the activation energy of R_{int}, at ~68kJ/mol has almost no change. However, the apparent activation energy for R_{chem} increases after aging from ~97kJ/mol to 115kJ/mol. This increase in the apparent activation energy of R_{chem} can be attributed to some permanent change in the surface of the LSCF, which becomes more pronounced at lower temperatures. Further investigation using *ex-situ* characterization techniques need to be performed to help determine possible mechanisms for the change in activation energy of R_{chem}.

The data obtained from EIS measurements on the effect of CO_2 for LSCF-GDC cells has been compared with ISTPX data under comparable conditions (15). Using ISTPX there is a strong interaction between CO_2 and LSCF across the entire temperature range explored (100-800°C). The exchange of CO_2 with LSCF tends to cause blocking of O_2 exchange sites, and under high concentrations of CO_2 can cause the formation of SrO (17, 24). From EIS data one can also see that the presence of CO_2 can change the oxygen reduction reaction, through an increase in the low frequency arc that we denote R_{chem}. Unlike CO_2, the interaction of H_2O appears to be dominant in the low temperature region, for both isotope exchange and EIS experiments.

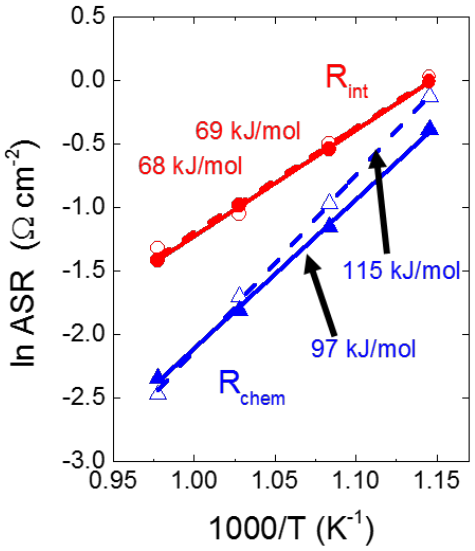

Figure 9. Arrhenius plots for LSCF-GDC cells before (closed symbols, solid lines) and after (open symbols, dashed lines). The activation energy of R_{chem} is affected by aging with the presence of 5% CO_2.

Conclusions

Electrochemical impedance spectroscopy was performed on composite LSCF-GDC cathodes to investigate the short-term and long-term effects of water and CO_2 on the ORR and cell performance. We have established a robust approach to de-convolute impedance data and extract meaningful quantities for the various contributions, i.e. the capacitance and resistance of individual components. The presence of 3% H_2O appears to increase the low frequency, chemical process of the ORR, especially as temperature decreases. However, despite the short-term effect of water at lower temperature, the long-term aging affects appear to be non-existent. To induce any changes in the LSCF-GDC cathode, it seems to be necessary to increase the operating temperature. The short-term effects of CO_2 are similar to those of H_2O. There is a definite increase in R_{chem} at both 450 and 750°C, but there are limited changes in the cell after low temperature aging. EIS results are in agreement with previously obtained data from gas phase isotopic oxygen exchange experiments.

Acknowledgements

The authors would like to acknowledge the support of the U.S. Department of Energy, SECA, Contract #: DEFE0009084. Thank you to the University of Maryland X-ray Crystallographic Center and NISPLab for use of their equipment.

References

1. E. D. Wachsman and K. T. Lee, *Science*, **334**, 935 (2011).
2. E. D. Wachsman, C. A. Marlowe and K. T. Lee, *Energy & Environmental Science*, **5**, 5498 (2012).
3. S. C. Singhal and K. Kendall, *High-temperature solid oxide fuel cells : fundamentals, design, and applicatons*, p. xvi, Elsevier Advanced Technology, New York (2003).
4. S. B. Adler, *Chemical reviews*, **104**, 4791 (2004).
5. S. Y. Lai, D. Ding, M. Liu, M. Liu and F. M. Alamgir, *ChemSusChem*, **7**, 3078 (2014).
6. D. W. S.J. Benson, and J.A. Kilner, *Journal of the Electrochemical Society*, **146**, 1305 (1999).
7. E. Bucher, W. Sitte, F. Klauser and E. Bertel, *Solid State Ionics*, **208**, 43 (2012).
8. R. R. Liu, S. H. Kim, S. Taniguchi, T. Oshima, Y. Shiratori, K. Ito and K. Sasaki, *Journal of Power Sources*, **196**, 7090 (2011).
9. Z. Zhao, L. Liu, X. Zhang, W. Wu, B. Tu, D. Cui, D. Ou and M. Cheng, *International Journal of Hydrogen Energy*, **38**, 15361 (2013).
10. S. B. Adler, J. A. Lane and B. C. H. Steele, *Journal of The Electrochemical Society*, **143**, 3554 (1996).
11. S. B. Adler, *Solid State Ionics*, **111**, 125 (1998).
12. F. Baumann, J. Fleig, H. Habermeier and J. Maier, *Solid State Ionics*, **177**, 1071 (2006).
13. B. A. Boukamp, N. Hildenbrand, P. Nammensma and D. H. A. Blank, *Solid State Ionics*, **192**, 404 (2011).
14. M. J. Jørgensen and M. Mogensen, *Journal of The Electrochemical Society*, **148**, A433 (2001).
15. Y. L. H. C. P. E. D. Wachsman, *in preparation* (2015).
16. D. Oh, D. Gostovic and E. D. Wachsman, *Journal of Materials Research*, **27**, 1992 (2012).
17. Y. Yu, H. Luo, D. Cetin, X. Lin, K. Ludwig, U. Pal, S. Gopalan and S. Basu, *Applied Surface Science*, **323**, 71 (2014).
18. P. Agarwal, M. E. Orazem and L. H. Garcia‐Rubio, *Journal of the Electrochemical Society*, **139**, 1917 (1992).
19. C. Xia and M. Liu, *Journal of the American Ceramic Society*, **84**, 1903 (2001).
20. B. C. H. Steele, *Solid State Ionics*, **129**, 95 (2000).
21. X. Guo, *Solid State Ionics*, **112**, 113 (1998).
22. H. Yokokawa, *Solid State Ionics*, **225**, 6 (2012).
23. M. J. Pietrowski, R. A. De Souza, M. Fartmann, R. ter Veen and M. Martin, *Fuel Cells*, **13**, 673 (2013).
24. Y. Orikasa, E. J. Crumlin, S. Sako, K. Amezawa, T. Uruga, M. D. Biegalski, H. M. Christen, Y. Uchimoto and Y. Shao-Horn, *ECS Electrochemistry Letters*, **3**, F23 (2014).